NIH Public Access
Author Manuscript
Nature. Author manuscript; available in PMC 2013 August 16.

Published in final edited form as:
Nature. 2012 August 16; 488(7411): 414–418. doi:10.1038/nature11267.

The Dynamic Disulfide Relay of Quiescin Sulfhydryl Oxidase

Assaf Alon[1], **Iris Grossman**[1], **Yair Gat**[1], **Vamsi K. Kodali**[2], **Frank DiMaio**[3], **Tevie Mehlman**[4], **Gilad Haran**[5], **David Baker**[3], **Colin Thorpe**[2], and **Deborah Fass**[1]

[1]Department of Structural Biology, Weizmann Institute of Science, Rehovot 76100, Israel

[2]Department of Chemistry and Biochemistry, University of Delaware, Newark, Delaware 19716, USA

[3]Department of Biochemistry, University of Washington, Seattle, Washington 98195, USA

[4]Department of Biological Research Support, Weizmann Institute of Science, Rehovot 76100, Israel

[5]Department of Chemical Physics, Weizmann Institute of Science, Rehovot 76100, Israel

Abstract

Protein stability, assembly, localization, and regulation often depend on formation of disulfide cross-links between cysteine side chains. Enzymes known as sulfhydryl oxidases catalyze *de novo* disulfide formation and initiate intra- and intermolecular dithiol/disulfide relays to deliver the disulfides to substrate proteins[1,2]. Quiescin sulfhydryl oxidase (QSOX) is a unique, multi-domain disulfide catalyst that is localized primarily to the Golgi apparatus and secreted fluids[3] and has attracted attention due to its over-production in tumors[4,5]. In addition to its physiological importance, QSOX is a mechanistically intriguing enzyme, encompassing functions typically carried out by a series of proteins in other disulfide formation pathways. How disulfides are relayed through the multiple redox-active sites of QSOX and whether there is a functional benefit to concatenating these sites on a single polypeptide are open questions. We determined the first crystal structure of an intact QSOX enzyme, derived from a trypanosome parasite. Notably, sequential sites in the disulfide relay were found more than 40 Å apart in this structure, too far for direct disulfide transfer. To resolve this puzzle, we trapped and crystallized an intermediate in the disulfide hand-off, which showed a 165° domain rotation relative to the original structure, bringing the two active sites within disulfide bonding distance. The comparable structure of a mammalian QSOX enzyme, also presented herein, reveals additional biochemical features that facilitate disulfide transfer in metazoan orthologs. Finally, we quantified the contribution of

To whom correspondence should be addressed: Deborah Fass, Dept. of Structural Biology, Weizmann Institute of Science, Rehovot 76100 Israel. Fax: +972-8-934-4136; deborah.fass@weizmann.ac.il.

Supplementary Information: is linked to the online version of the paper at www.nature.com/nature.

Author Contributions: A.A. designed experiments, expressed, purified, and crystallized proteins, and, together with D.F., solved and refined the TbQSOX, TbQSOX$_C$, and MmQSOX1$_C$ structures. A.A. also performed the FRET and cross-linking experiments. I.G. improved the TbQSOX crystals. Y.G. grew the MmQSOX1$_C$ crystals. V.K. and C.T. provided plasmids and helped design and analyze experiments. F.D. and D.B. accomplished molecular replacement to solve the HsQSOX1(PDI) structure. T.M. performed the mass spectrometry experiments and analyses. G.H. helped design and analyze the FRET experiments and assisted with operation of the fluorimeter. D.F. expressed proteins, performed oxygen consumption measurements, and designed and analyzed experiments. A.A. and D.F. wrote the manuscript.

Atomic coordinates and structure factors for the TbQSOX, TbQSOX$_C$, and HsQSOX1(PDI) structures have been deposited with the Protein Data Bank (http://www.rcsb.org) under accession codes 3QCP, 3QD9, 3Q6O, respectively. The MmQSOX1$_C$ coordinates and structure factors have been deposited with accession codes 3T58 (orthorhombic) and 3T59 (monoclinic). Reprints and permissions information is available at www.nature.com/reprints

The authors declare no competing financial interests

$watermark-text
$watermark-text
$watermark-text

concatenation to QSOX activity, providing general lessons for the understanding of multi-domain enzymes and the design of novel catalytic relays.

The introduction of disulfide bonds into folding proteins is typically accomplished by enzyme pairs[1,2]. One enzyme generates disulfides *de novo*, often with the aid of a bound cofactor. The second enzyme acquires these disulfides by dithiol/disulfide exchange and passes them to substrate proteins. Examples of such partnerships are DsbB and DsbA in the *E. coli* periplasm, Ero1 and PDI in the endoplasmic reticulum (ER), and Erv1 and Mia40 in the mitochondrial intermembrane space. A partnership between VKOR and membrane-anchored PDI-family proteins has also been identified in the ER[6]. The QSOX enzymes[3] are the only known example for conserved concatenation of disulfide generating and disulfide transferring modules within a single polypeptide (Fig. 1a), though a VKOR-like protein is fused to its partner in a few species[7]. Domain fusion may allow QSOX to function under dilute conditions in extracellular environments[8–10]; other disulfide generating enzymes function in sequestered intracellular compartments with high local concentrations of disulfide transferring enzymes.

Formation and transfer of disulfide bonds in QSOX are mediated by redox-active cysteine pairs in the canonical pattern Cys-X-X-Cys (Fig. 1a). One such di-cysteine motif is in a thioredoxin-fold domain (Trx1) related to the redox-active domains of PDI. Another is in a flavin adenine dinucleotide (FAD) binding domain related to the mitochondrial Erv1 (Erv). The proposed QSOX mechanism[11,12], involves generation of disulfides catalytically at the FAD-proximal di-cysteine motif, intramolecular disulfide transfer to the Trx1 domain, and finally intermolecular dithiol/disulfide exchange with substrate (Fig. 1a). An outstanding question is how the Trx1 redox-active residues interact alternately with the Erv domain and with substrate proteins.

The *Trypanosoma brucei* parasite, cause of African trypanosomiases, encodes a QSOX enzyme (TbQSOX)[13]. We determined the X-ray crystal structure of TbQSOX to 2.3 Å resolution (Supplementary Table I). In the crystallized configuration, the Trx1 redox-active site faces outwards (Fig. 1b), where it would be readily accessible to nucleophilic attack by substrate cysteine thiolates. However, in this position, the Trx1 active site is 42 Å away from the Erv active site and would thus be unable, after disengaging from substrate, to accomplish the next step in the proposed relay mechanism (Fig. 1a).

To test whether the distance between redox-active sites in the TbQSOX crystal structure is representative of their average separation in solution, we used fluorescence resonance energy transfer (FRET) spectroscopy. TbQSOX Cys72 was mutated to leave one cysteine (Cys69) free within the Trx1 active site for labeling with the donor fluorophore Pacific Blue C5-maleimide (Invitrogen). The bound FAD, though not fluorescent, served as an energy acceptor at the Erv active site, and decrease in donor fluorescence was taken to reflect FRET efficiency. Use of an intrinsic chromophore as one member of the FRET pair minimized potential perturbations due to labeling. An average distance of 55 Å was calculated between the label at position 69 and the FAD (Supplementary Table II), supporting a requirement for significant conformational changes during the QSOX disulfide relay. Donor label introduced at a variety of other positions across the enzyme surface provided a set of ensemble-averaged distances characterizing the resting state of the enzyme (Fig. 1c, Supplementary Figs. 1–3, Supplementary Tables II and IIIa, b, c).

To obtain structural insight into the intramolecular disulfide transfer step (see Supplementary Discussion), we eliminated the second cysteine of both TbQSOX redox-active Cys-X-X-Cys motifs. The resulting mutant is able to form, but not resolve, the interdomain disulfide essential for catalysis. We purified (Supplementary Fig. 4) and

$watermark-text $watermark-text $watermark-text

$watermark-text

$watermark-text

$watermark-text

crystallized the closed, interdomain disulfide-bonded version of TbQSOX ($TbQSOX_C$) and solved its structure to 3.3 Å resolution. When compared with the wild-type enzyme, a ~165° rotation of the Trx1 domain and associated helix brings the two redox-active sites within covalent bonding distance in $TbQSOX_C$ (Fig. 1d; Supplementary Movie 1). Consistent with this closed configuration being a transient state during enzyme turnover, the surface complementarity between $TbQSOX_C$ redox- active domains is greater than non-evolved interfaces (*i.e.*, crystal contacts) and less than stable protein-protein interactions[14].

In addition to illustrating the functionally important re-orientation of the redox-active sites, the $TbQSOX_C$ structure shows how closure of the Trx1 domain over the FAD-binding site may enhance the active-site chemistry for disulfide formation. In the reduced, anionic form of flavin, negative charge is distributed over atoms N1, O2, and O4 of the isoalloxazine. Other disulfide-forming enzymes position a basic residue near the cofactor to stabilize this negative charge[15,16]. In $TbQSOX_C$, the Trx1 domain contributes an arginine side chain (Arg74) as an interaction partner for the FAD O2 atom (Fig. 1e), which may promote formation of a thiol-flavin charge-transfer complex and in turn a reduced state of the FAD. Indeed, the TbQSOX Arg74Ala mutant is substantially less active than wild type (Supplementary Fig. 5). Other basic residues within the Erv domain (*i.e.*, His356 and Arg382) may further modulate the electrostatic environment of the FAD.

A second FRET study was conducted, this time monitoring energy transfer kinetically in the presence of substrate. The TbQSOX mutant with donor fluorophore at residue 160 (Supplementary Table IIIc) showed a reproducible FRET increase when substrate was added (Fig. 2a). As expected, when oxygen was not limiting the FRET signal returned to resting values as substrate was exhausted (Fig. 2b). These observations indicate that the labeled position is closer to the FAD in cycling TbQSOX than in the resting, native ensemble, further supporting conformational changes during catalysis.

Though TbQSOX has conserved functional features characteristic of the QSOX family, it is one of the most divergent orthologs. TbQSOX lacks a domain (Trx2) found in metazoan QSOX enzymes (Fig. 1a), and its Trx1 redox-active motif, Cys-Gly-Ala-Cys, differs from the Cys-Gly-His-Cys common to other QSOXs and to PDI-family proteins. We therefore expanded our study to include the architecture and dynamics of mammalian QSOXs.

The structure of *Homo sapiens* QSOX1 (HsQSOX1) was solved in two complementary fragments, HsQSOX1(PDI) and HsQSOX1(Erv) (Fig. 1a), crystallized separately (Fig. 3a, Supplementary Fig. 6, and ref. 17). The HsQSOX1 domains containing redox-active Cys-X-X-Cys motifs were found to be similar to their TbQSOX counterparts (Supplementary Table IV). Outside these regions, the human and parasite structures are more divergent. In particular, HsQSOX1 has the Trx2 domain but lacks the long helix of TbQSOX (Fig. 1b). The two functional modules of HsQSOX1 appear to be flexibly tethered to one another as found for TbQSOX (Supplementary Table V, Supplementary Fig. 7).

Mammalian QSOX mutants designed to mimic the interdomain disulfide transfer intermediate, analogous to $TbQSOX_C$, were then constructed. The *Mus musculus* structure, $MmQSOX1_C$, solved to 2.4 Å resolution, demonstrated how disulfide transfer readily accommodates the additional domain in metazoan QSOX (Fig. 3b). Moreover, some features that may orient the two enzyme halves are conserved (Supplementary Figs. 8,9). One difference between $TbQSOX_C$ and $MmQSOX1_C$, however, is the presence of the histidine (His75) in the MmQSOX1 Trx1 Cys-Gly-His-Cys motif. His75 appeared in two distinct rotamers in the $MmQSOX1_C$ crystals, providing insight into the dynamics of catalysis (Supplementary Figs. 10,11). In one configuration, His75 would be in position to transiently interact with the thiolate of the Erv active-site cysteine Cys452 during resolution

$watermark-text

$watermark-text

$watermark-text

of the interdomain disulfide intermediate (Supplementary Fig. 11). A comparison of HsQSOX1(PDI) with $MmQSOX1_C$ reveals how the end of the Trx1 redox-active helix rearranges upon interaction with the FAD-binding domain (Fig. 3c). No Trx1 side chain comparable to TbQSOX Arg74 interacts with the flavin in $MmQSOX1_C$, but unpaired NH groups at the amino terminus of the $MmQSOX1_C$ Trx1 redox-active helix approach the FAD O2 (Fig. 3c). Furthermore, Arg490 is recruited from within the Erv domain for interaction with FAD O4 (Supplementary Fig. 11), like its corresponding residue in TbQSOX (Arg382). In summary, many structural and dynamics properties of mammalian and trypanosome QSOXs are similar, and both enzymes appear to recruit electron-withdrawing groups to modulate active-site electrostatics during catalysis. However, the mammalian QSOX crystal structures reveal for the first time the plasticity and sophistication of the Cys-Gly-His-Cys motif, present in numerous redox-active proteins of the PDI family[18].

The expansion of multi-domain protein architectures contributes to the growth of the protein universe[19] and the development of complex species[20]. In few cases, however, is it possible to determine quantitatively how domain fusion contributes to protein function. QSOX, due to its modular structure, provides an opportunity to quantify the benefit of concatenation of functional units. We measured the extent of this benefit by adding increasing concentrations of HsQSOX1(PDI) to catalytic amounts of HsQSOX1(Erv) to determine the ratio necessary to achieve the reaction rate of intact HsQSOX1 (Fig. 3d). We observed that the effective concentration of the disulfide transferring module is increased more than 2500-fold by its concatenation to the disulfide generating module *via* a poorly conserved linker (Supplementary Fig. 12). Our results emphasize the principle, applicable to design and *in vitro* evolution of novel catalytic or signaling relays, that the function of proteins acting in tandem may be greatly improved by concatenation using flexible, generic linkers.

Although mammalian cells are replete with PDI-family proteins[18], which contain diverse numbers and arrangements of redox-active and -inactive domains, QSOX is the only enzyme with an oxidoreductase domain homologous to PDI fused to a domain that generates disulfide bonds *de novo*. QSOX is also exceptional in exhibiting a primary localization outside the ER. The QSOX structures reported here show how the two functions of the enzyme, generation of disulfides and transfer to substrate proteins, are permitted through a loose tethering of the two modules (Fig. 3e). On one hand, the fusion is sufficient to greatly increase the effective concentration of the two active sites, but on the other it allows an enormous range of motion. Understanding how this flexibility may further contribute to interactions with substrate must await identification of the native targets of QSOX catalysis in the late secretory pathway and extracellular environment.

METHODS

Plasmid construction

TbQSOX mutants not previously available were made using the Quikchange mutagenesis kit (Stratagene) on the basis of the published TbQSOX expression plasmid[13]. HsQSOX1(PDI) spans residues 33 to 272 of *Homo sapiens* QSOX1. The coding sequence for this region was cloned between the NdeI and BamHI sites of the pET-15b vector (Novagen). The HsQSOX1 protein used for activity assays spans residues 33 to 546 of *Homo sapiens* QSOX1. The coding sequence for this region was cloned between the NdeI and BamHI sites of the pET-15b vector (Novagen). The thrombin cleavage site and His_6 tag encoded by the vector were excised by NcoI and NdeI restriction and replaced with a His_6 tag only. The MmQSOX1 Cys76Ala/Cys455Ser double-mutant was made by mutation of a *Mus musculus* synthetic QSOX1 gene codon-optimized for protein production in *E. coli* (Genescript). The

$watermark-text

$watermark-text

$watermark-text

coding sequence for residues 36 to 550 was inserted into pET-15b between the NdeI and BamH1 sites.

Protein preparation

TbQSOX and its mutants were produced in the Origami 2 (DE3) *E. coli* cell strain as described[13] except that bacteria were grown in LB media. The MmQSOX1 Cys76Ala/Cys455Ser double mutant was produced in the BL21 (DE3) plysS strain. Cells were lysed by sonication in 20 mM sodium phosphate buffer, pH 7.4, 500 mM NaCl, 20 mM imidazole, supplemented with protease inhibitors (100 μg/ml phenylmethanesulfonylfluoride (PMSF), 1 μg/ml each of leupeptin, aprotinin, pepstatin A). Crude extract was clarified by centrifugation at 40,000×g for 1 hr. The enzymes, containing amino-terminal His_6 tags, were purified from the soluble fraction by Ni-NTA chromatography (GE Healthcare). Eluted TbQSOX, TbQSOX mutants, and the MmQSOX1 mutant were exchanged into 20 mM sodium phosphate buffer, pH 7.4, 100 mM NaCl, 20 mM imidazole using a PD-10 desalting column (GE Healthcare). Thrombin (10 units/mg protein) was added, and the cleavage reaction was incubated for 2 hours at room temperature. PMSF was added to 1 mM to inhibit the thrombin, and the protein was re-applied to Ni-NTA resin. Unbound material was collected, concentrated, applied to a PD-10 desalting column pre-equilibrated with crystallization stock buffer (10 mM Tris, pH 8, 100 mM NaCl), and then applied to a HiLoad 16/60 Superdex 75 gel filtration column (GE Healthcare) under the same buffer conditions. Alternatively, size exclusion chromatography was performed in 20 mM sodium phosphate buffer, pH 7.5, 200 mM NaCl. The Cys72Ser/Cys353Ser TbQSOX mutant was incubated prior to gel filtration with maleimide-functionalized polyethylene glycol (PEG) of molecular weight 5 kD. The Cys76Ala/Cys455Ser MmQSOX1 mutant was incubated with maleimide-functionalized PEG of molecular weight 10 kD. The fraction lacking the Cys69-Cys350 disulfide bond (for TbQSOX) or the Cys73-Cys452 disulfide bond (for MmQSOX1) became doubly modified by PEG, which increased its hydrodynamic radius sufficiently to allow separation from $TbQSOX_C$ or $MmQSOX1_C$ (Supplementary Fig. 4). Due to high yields of the MmQSOX1 mutant, the peak corresponding to the protein not modified by PEG was collected, re-concentrated, and loaded again on the gel filtration column to achieve complete separation from PEG-modified material.

HsQSOX1, HsQSOX1(PDI), and HsQSOX1(Erv) were produced in the BL21 (DE3) plysS *E. coli* cell strain and purified as for wild-type TbQSOX, except that the HsQSOX1 construct lacked a thrombin cleavage site so was subjected to gel filtration after the first Ni-NTA column without the cleavage step. Prior to crystallization, HsQSOX1(PDI) was treated with dimethylamine-borane complex to methylate lysines as described[21], and the protein was then separated from excess reagents by gel filtration in crystallization stock buffer.

Protein crystallization

Crystals were grown by hanging-drop vapor diffusion at 293 K. Wild-type TbQSOX and Ser160Cys TbQSOX crystals were grown over a well solution containing 14–18% w/v PEG 2 kD monomethyl ether (MME), 10% v/v ethylene glycol. Crystals were transferred to a solution containing 20% w/v PEG 2 kD MME, 20% v/v ethylene glycol, then transferred to a 1:1 mixture of mineral oil and Paratone (Exxon) oil before flash freezing. Crystals of $TbQSOX_C$ were grown over a well solution containing 20% w/v PEG 3.35 kD, 0.2 M sodium sulfate, 0.5% w/v polyvinylpyrrolidone K15. Crystals were transferred to a solution of 25% v/v glycerol, 0.2 M sodium sulfate, 20% w/v PEG 3.35 kD and flash frozen. Crystals of the methylated HsQSOX1(PDI) were grown over a well solution containing 20% w/v PEG 3.35 kD, 0.2 M lithium sulfate monohydrate. Crystals were transferred to a solution of 25% v/v glycerol, 20% w/v PEG 3.35 kD, 0.2 M lithium sulfate monohydrate and flash frozen. Crystals of $MmQSOX1_C$ grown over a well solution containing 0.1 M 2-(N-

morpholino)ethanesulfonic acid (MES) buffer, pH 6.5, 12% w/v PEG 20 kD were of the orthorhombic space group $P2_12_12_1$. These crystals were transferred to a solution of 0.1 M MES, pH 6.5, 12% w/v PEG 20 kD, 25% v/v glycerol for freezing. Crystals of $MmQSOX1_C$ grown over a well solution containing 0.1 M 2-[4-(2-hydroxyethyl)piperazin-1-yl]ethanesulfonic acid (HEPES) buffer, pH 7.0, 10% v/v 1,5-pentanediol, 5% v/v glycerol were of the monoclinic space group $P2_1$. These crystals were first transferred to a solution of 0.1 M HEPES, pH 7.0, 10% v/v 1,5-pentanediol, 25% v/v glycerol, and then transferred to a 1:1 mixture of mineral oil and Paratone oil for freezing.

Data collection

Diffraction data were collected at 100 K. Data for wild-type TbQSOX crystals, HsQSOX1(PDI), and the monoclinic ($P2_1$) $MmQSOX1_C$ crystals were collected at a wavelength of 1.544 Å on a RU-H3R generator (Rigaku) equipped with a RaxisIV++ image plate system and Osmic mirrors. TbQSOX data were collected to 2.3 Å resolution from crystals of space group $P2_12_12$. Data for the HsQSOX1(PDI) were collected to 2.05 Å resolution from a crystal of space group $P2_12_12_1$. Data for monoclinic $MmQSOX1_C$ were collected to 2.8 Å resolution from a crystal of space group $P2_1$. Data from the $TbQSOX_C$ crystals, of space group $P2_1$, were collected at a wavelength of 0.9769 Å to 3.3 Å resolution on ESRF beamline ID23-1 using a helical data collection strategy (for rod-shaped crystals). Data for orthorhombic ($P2_12_12_1$) $MmQSOX1_C$ were collected at a wavelength of 1.000 A to 2.4 Å resolution on ESRF beamline ID29. Data for TbQSOX Ser160Cys crystals were collected at a wavelength of 1.005 Å to 2.6 Å resolution on ESRF beamline BM30. Data from TbQSOX, TbQSOX Ser160Cys, $MmQSOX1_C$ monoclinic, and $MmQSOX1_C$ orthorhombic crystals were processed and scaled using DENZO and SCALEPACK[23]. $TbQSOX_C$ and HsQSOX1(PDI) data were processed and scaled using iMOSFLM[24] and SCALA[25].

Structure solution

The wild-type TbQSOX structure was determined by molecular replacement (MR) using Phaser[26]. The helical core of the partial human QSOX structure (PDB code 3LLK) and a homology model of the TbQSOX Trx1 domain generated using Modeller[27] were used as search models. The $TbQSOX_C$ structure was determined by MR using fragments of the wild-type TbQSOX structure as search models in Phaser. The HsQSOX1(PDI) structure was determined by MR, using search models from yeast Mpd1p (PDB code 3ED3) and K53E thioredoxin from *Sulfolobus tokodaii* (PDB code 2E0Q). A template based on 3ED3, trimmed of non-conserved loops and sidechains, was first placed using Phaser; gaps in the template were rebuilt and refined using density- and energy-guided optimization with Rosetta[22]. This allowed placement of the second domain by Phaser, using a trimmed model based on 2E0Q, which underwent the same rebuilding procedure. Model refinement was performed using CNS[28] or Phenix[29] incorporating the TLSMD[30] procedure. In all cases, model rebuilding was done using Coot[31]. The $MmQSOX1_C$ structure was determined using the $P2_12_12_1$ data and the structures of HsQSOX1(PDI) and HsQSOX1(Erv) as search models in Phaser. Chain A of the refined $MmQSOX1_C$ model was positioned (four copies) in the $P2_1$ $MmQSOX1_C$ crystal unit cell using Phaser and further refined using CNS[28]. As assessed using MolProbity[32], there are no Ramachandran outliers in the structures reported herein.

Surface complementarity

Normalized interface packing (NIP) and normalized surface complementarity (NSc) were calculated according to Mitra and Pal[33]. The interface area between the Trx1 domain and the ψErv/Erv domains in $TbQSOX_C$ was calculated to be 867 $Å^2$. The NIP and NSc values were calculated to be 2.33×10^{-4} and 3.87×10^{-4}, respectively. The interface area between

$watermark-text $watermark-text $watermark-text

$watermark-text

$watermark-text

$watermark-text

the comparable domains of $MmQSOX1_C$ was calculated to be 892 $Å^2$. The NIP and NSc values were calculated to be 2.49×10^{-4} and 3.70×10^{-4}, respectively. The QSOX NIP values are greater than ~75% of the NIP values for evolved complexes and less than ~85% of the NIP values for crystal contacts of monomeric proteins. The QSOX NSc values are greater than ~80% of the NSc values for evolved complexes and less than 83% of the NSc values for crystal contacts. For comparison, the interface area of the two subunits in the Erv2p dimer (1JR8) was calculated to be 1233 $Å^2$, and the NIP and NSc values were 1.81×10^{-4} and 2.30×10^{-4}, respectively. The Erv2p NIP value is greater than 39% of the NIP values for evolved complexes (*i.e.*, squarely within the expected packing values for complexes) and less than 95% of the NIP values for crystal contacts (*i.e.*, the packing is much better than most crystal contacts). The Erv2p NSc value is greater than 57% of the NSc values for evolved complexes (*i.e.*, the surface complementarity is typical of evolved complexes) and less than ~94% of the NSc values for crystal contacts (*i.e.*, the complementarity is much better than for most crystal contacts).

Fluorescence resonance energy transfer spectroscopy

All mutants used for FRET studies were purified as for the wild-type enzymes except that a 5- to 10-fold molar excess of C5-Pacific Blue maleimide (Invitrogen) was added after gel filtration. A second gel filtration was then performed to remove excess dye. The fraction corresponding to the peak of the gel filtration chromatogram was used for further study. FRET experiments were performed in a 1 cm pathlength cuvette at a protein concentration of 6.3 nM in 20 mM sodium phosphate buffer, pH 7.5, 200 mM NaCl, 0.5 mM EDTA. Excitation was at a wavelength of 400 nm. As the fluorescence acceptor, namely the bound FAD cofactor, is an intrinsic part of QSOX enzymes, quantum yield of fluorophore conjugated at various positions in the native protein in the absence of acceptor could not be directly determined. Instead, acceptor absorbance was diminished *in situ* by reduction to $FADH_2$, which results in an 83% decrease in absorbance at 454 nm. Reduction was accomplished by the addition of glucose oxidase and glucose to deplete the dissolved oxygen, and DTT to reduce the TbQSOX active site as described in Supplementary Fig. 3. Donor fluorescence was monitored kinetically until an abrupt increase was observed, indicating conversion to $FADH_2$. Reduced state wavelength scans were then collected. Distances were calculated as described in Supplementary Table II.

Mass spectrometry

Gel fragments were treated with varying protease combinations at 37 °C in 50 mM ammonium bicarbonate. Peptide mixtures were extracted from the gels with 80% CH_3CN, 1% CF_3COOH, and the organic solvent was evaporated in a vacuum centrifuge. The resulting peptide mixtures were reconstituted in 80% formic acid and immediately diluted 1:10 with Milli-Q water prior to mass spectrometry analysis. Tandem mass spectrometry (LC-MS/MS) was performed using a 15 cm reversed phase spraying fused-silica capillary column (inner diameter 75 μm) made in-house and packed with 3 μm ReproSil-Pur C_{18}AQ media (Dr. Maisch GmbH, Ammerbuch-Entringen, Germany) using an UltiMate3000 Capillary/Nano LC System (LC Packings, Dionex). The LC system was used in conjunction with an LTQ Orbitrap (Thermo Fisher Scientific) operated in the positive ion mode and equipped with a nanoelectrospray ion source. Peptides were separated with a 50 min gradient from 5 to 65% acetonitrile (buffer A: 5% acetonitrile, 0.1% formic acid, 0.005% TFA; buffer B: 90% acetonitrile, 0.2% formic acid, 0.005% TFA). The voltage applied to the union in order to produce an electrospray was 1.2 kV. The mass spectrometer was operated in the data-dependent mode. Survey MS scans were acquired in the Orbitrap with the resolution set to a value of 60,000. Up to the six most intense ions per scan were fragmented and analyzed in the linear trap. For the analysis of peptides, survey scans were recorded in the FT-mode followed by data-dependent collision-induced dissociation (CID)

of the six most intense ions in the linear ion trap (LTQ). Raw data files were searched with MASCOT (Matrix Science, London, UK) against a Swissprot database modified by inclusion of the relevant mutants. The program MassMatrix[34] was used for identification of disulfide bonds and BS3 cross-links from MGF files.

QSOX enzyme assays

Sulfhydryl oxidase activity was measured at 25 °C by monitoring oxygen consumption in a Clarke-type oxygen electrode (Hansatech Instruments Ltd.). Buffer conditions were 50 mM potassium phosphate buffer, pH 7.5, 300 mM NaCl, 1 mM EDTA. HsQSOX1(PDI) and HsQSOX1(Erv) were mixed in the oxygen electrode chamber, and reactions were initiated by injection of DTT to a concentration of 1 mM. For comparison, *E. coli* thioredoxin was prepared as described[35] and used in place of HsQSOX1(PDI). Intact HsQSOX1 activity was remeasured[12] for reference by diluting the enzyme to 100 nM into the oxygen electrode chamber and initiating the reaction by injection of DTT to 1 mM. Turnover numbers were calculated per FAD cofactor. Oxygen consumption by HsQSOX1(Erv) alone is indistinguishable from background rates under these conditions (not shown). Oxygen consumption in the presence of varying concentrations of HsQSOX1(PDI) alone or thioredoxin alone is minimal.

Supplementary Material

Refer to Web version on PubMed Central for supplementary material.

Acknowledgments

Shelly Rogotner and Orly Dym from the Israel Structure Proteomics Center helped in growing the $TbQSOX_C$ crystals. We thank Tal Ilani and Amnon Horovitz for critical reading of the manuscript, and Nathan Nelson and his research group for help with X-ray data collection. Adi Moseri assisted with HPLC. This study was funded by the Israel Science Foundation. D.F. and A.A. acknowledge the Kimmelman Center for Macromolecular Assemblies for additional support. C.T. and V.K. acknowledge NIH grant GM26643. The molecular movie was produced using the UCSF Chimera package from the Resource for Biocomputing, Visualization, and Informatics at the University of California, San Francisco (supported by NIH P41 RR001081).

References

1. Riemer J, Bulleid N, Herrmann JM. Disulfide formation in the ER and mitochondria: two solutions to a common process. Science. 2009; 324:1284–1287. [PubMed: 19498160]
2. Tu BP, Weissman JS. Oxidative protein folding in eukaryotes: mechanisms and consequences. J Cell Biol. 2004; 164:341–346. [PubMed: 14757749]
3. Kodali VK, Thorpe C. Oxidative protein folding and the quiescin-sulfhydryl oxidase family of flavoproteins. Antiox Redox Signal. 2010; 13:1217–1230.
4. Antwi K, et al. Analysis of the plasma peptidome from pancreas cancer patients connects a peptide in plasma to overexpression of the parent protein in tumors. J Proteome Res. 2009; 8:4722–4731. [PubMed: 19795908]
5. Song H, et al. Loss of Nkx3.1 leads to the activation of discrete downstream target genes during prostate tumorigenesis. Oncogene. 2009; 28:3307–3319. [PubMed: 19597465]
6. Schulman S, Wang B, Li W, Rapoport TA. Vitamin K epoxide reductase prefers ER membrane-anchored thioredoxin-like redox partners. Proc Natl Acad Sci USA. 2010; 107:15027–15032. [PubMed: 20696932]
7. Goodstadt L, Ponting CP. Vitamin K epoxide redutase: homology, active site and catalytic mechanism. Trends Biochem Sci. 2004; 29:289–292. [PubMed: 15276181]
8. Zanata SM, et al. High levels of active quiescin Q6 sulfhydryl oxidase (QSOX) are selectively present in fetal serum. Redox Rep. 2005; 10:319–323. [PubMed: 16438804]

$watermark-text
$watermark-text
$watermark-text

$watermark-text

$watermark-text

$watermark-text

9. Ostrowski MC, Kistler WS. Properties of a flavoprotein sulfhydryl oxidase from rat seminal vesicle secretion. Biochem. 1980; 19:2639–2645. [PubMed: 7397095]
10. Jaje J, et al. A flavin-dependent sulfhydryl oxidase in bovine milk. Biochem. 2007; 46:13031–13040. [PubMed: 17944490]
11. Raje S, Thorpe C. Inter-domain redox communication in flavoenzymes of the quiescin/sulfhydryl oxidase family: role of a thioredoxin domain in disulfide bond formation. Biochem. 2003; 42:4560–4568. [PubMed: 12693953]
12. Heckler EJ, Alon A, Fass D, Thorpe C. Human quiescin-sulfhydryl oxidase, QSOX1: probing internal redox steps by mutagenesis. Biochem. 2008; 47:4955–4963. [PubMed: 18393449]
13. Kodali VK, Thorpe C. Quiescin sulfhydryl oxidase from *Trypanosoma brucei*: catalytic activity and mechanism of a QSOX family member with a single thioredoxin domain. Biochem. 2010; 49:2075–2085. [PubMed: 20121244]
14. Mitra P, Pal D. New measures for estimating surface complementarity and packing at protein-protein interfaces. FEBS Lett. 2010; 584:1163–1168. [PubMed: 20153323]
15. Inaba K, Takahashi Y-h, Ito K, Hayashi S. Critical role of a thiolate-quinone charge transfer complex and its adduct form in *de novo* disulfide bond generation by DsbB. Proc Natl Acad Sci USA. 2006; 103:287–292. [PubMed: 16384917]
16. Fass D. The Erv family of sulfhydryl oxidases. Biochim Biophys Acta. 2008; 1783:557–566. [PubMed: 18155671]
17. Alon A, Heckler EJ, Thorpe C, Fass D. QSOX contains a pseudo-dimer of functional and degenerate sulfhydryl oxidase domains. FEBS Lett. 2010; 584:1521–1525. [PubMed: 20211621]
18. Appenzeller-Herzog C, Ellgaard L. The human PDI family: versatility packed into a single fold. Biochim Biophys Acta. 2008; 1783:535–548. [PubMed: 18093543]
19. Levitt M. Nature of the protein universe. Proc Natl Acad Sci USA. 2009; 106:11079–11084. [PubMed: 19541617]
20. Tordai H, Nagy A, Farkas K, Banyai L, Patthy L. Modules, multidomain proteins and organismic complexity. FEBS J. 2005; 272:5064–5078. [PubMed: 16176277]
21. Walter TS, et al. Lysine methylation as a routine rescue strategy for protein crystallization. Structure. 2006; 14:1617–1622. [PubMed: 17098187]
22. Dimaio F, et al. Improved molecular replacement by density- and energy-guided protein structure optimization. Nature. 2011; 473:540–543. [PubMed: 21532589]
23. Otwinowski Z, Minor W. Processing of X-ray diffraction data collected in oscillation mode. Methods Enzymol. 1997; 276:307–326.
24. Leslie AGW. Recent changes to the MOSFLM package for processing film and image plate data. Joint CCP4 + ESF-EAMCB Newsletter on Protein Crystallography. 1992; 26:27–33.
25. Evans PR. Scaling and assessment of data quality. Acta Cryst D. 2005; 62:72–82. [PubMed: 16369096]
26. McCoy AJ, et al. *Phaser* crystallographic software. J Appl Crystallogr. 2007; 40:658–674. [PubMed: 19461840]
27. Eswar N, Eramian D, Webb B, Shen MY, Sali A. Protein structure modeling with MODELLER. Meth Mol Biol. 2008; 426:145–159.
28. Brunger AT, et al. Crystallography & NMR system: A new software suite for macromolecular structure determination. Acta Crystallogr D. 1998; 54:905–921. [PubMed: 9757107]
29. Afonine PV, Grosse-Kunstleve RW, Adams PD. The Phenix refinement framework. CCP4 Newsletter. 2005; 42 contribution 8.
30. Painter J, Merritt EA. Optimal description of a protein structure in terms of multiple groups undergoing TLS motion. Acta Crystallogr D. 2006; 62:439–450. [PubMed: 16552146]
31. Emsley P, Cowtan K. Coot: model-building tools for molecular graphics. Acta Crystallogr D. 2005; 60:2126–2132. [PubMed: 15572765]
32. Chen VB, et al. MolProbity: all-atom structure validation for macromolecular crystallography. Acta Crystallogr D. 2010; 66:12–21. [PubMed: 20057044]
33. Mitra P, Pal D. New measures for estimating surface complementarity and packing and protein-protein interfaces. FEBS Lett. 2010; 584:1163–1168. [PubMed: 20153323]

34. Xu H, Zhang L, Freitas MA. Identification and characterization of disulfide bonds in proteins and peptides from tandem MS data by use of the MassMatrix MS/MS search engine. J Proteome Res. 2008; 7:138–144. [PubMed: 18072732]

35. Gross E, et al. Generating disulfides enzymatically: reaction products and electron acceptors of the endoplasmic reticulum thiol oxidase Ero1p. Proc Natl Acad Sci USA. 2006; 103:299–304. [PubMed: 16407158]

$watermark-text

$watermark-text

$watermark-text

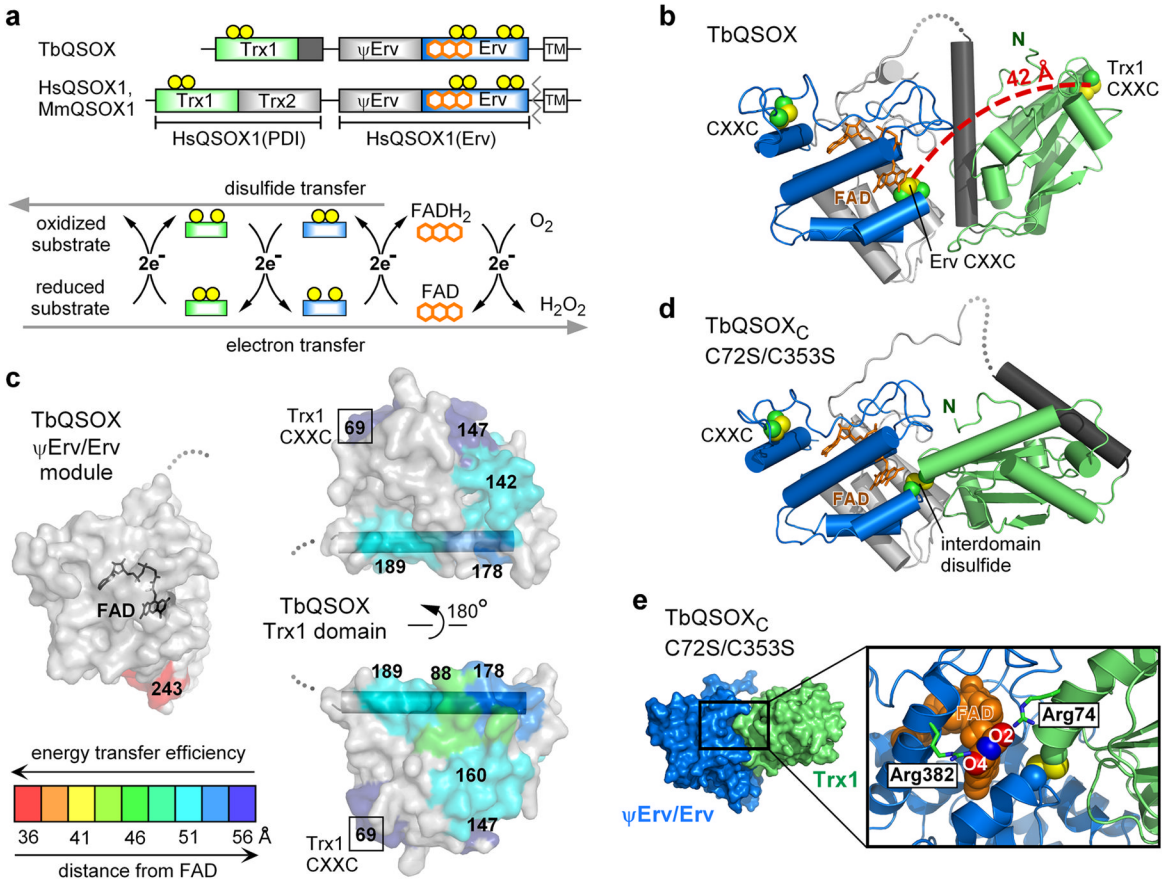

Figure 1. TbQSOX undergoes domain re-orientation to accomplish disulfide relay

a, CXXC motifs are illustrated as pairs of yellow balls in maps of trypanosome and mammalian QSOX enzymes. Other cysteines are shown in Supplementary Fig. 13. Fused hexagons represent the FAD cofactor. A degenerate Erv-like domain[17] is designated "ψErv". Arrows depict the electron transfer relay from reduced substrates to molecular oxygen and the corresponding outward flow of disulfide equivalents from QSOX to its substrates. **b**, TbQSOX structure colored according to **a**. Disulfides in CXXC motifs are in space filling representation (Cβ atom green, sulfur yellow). Structure stereo views are in Supplementary Fig. 14. **c**, Color-coded intramolecular distances between fluorophore-labeled TbQSOX cysteines and the bound FAD cofactor. **d**, Structure of $TbQSOX_C$. **e**, Surface representation of $TbQSOX_C$ and zoom into the interdomain interface. FAD is in space-filling representation with oxygen atoms (red) labeled. Structure figures were made using PyMOL (http://www.pymol.org).

$watermark-text
$watermark-text
$watermark-text

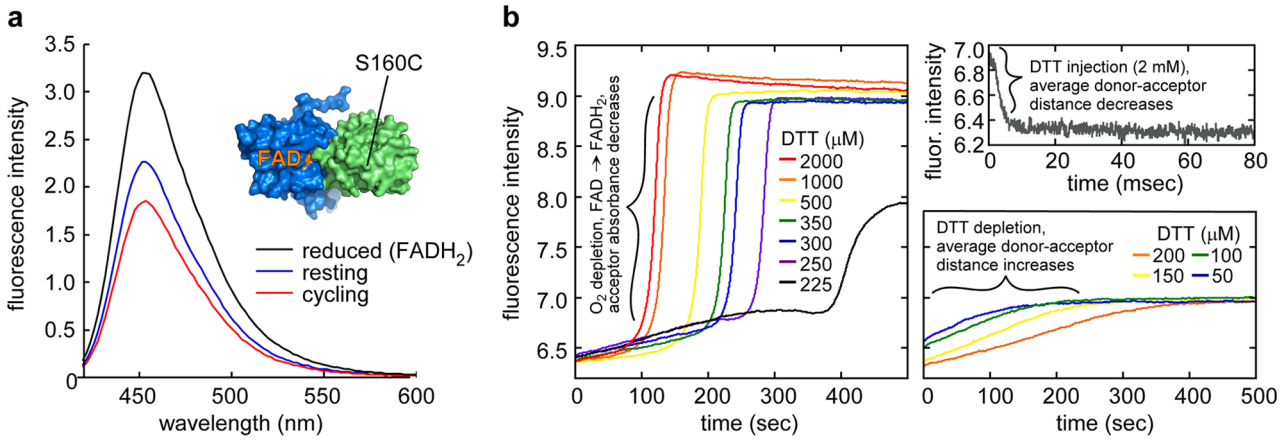

Figure 2. Changes in the TbQSOX conformational ensemble during catalysis

a, Fluorescence of Pacific Blue conjugated at position 160 in resting TbQSOX (blue), TbQSOX oxidizing the model substrate dithiothreitol (DTT) (red), and upon oxygen depletion and conversion of the energy acceptor FAD to $FADH_2$ (black). Inset, surface representation of $TbQSOX_C$, as in Fig. 1e, with FAD and donor labeling site indicated. **b**, Kinetics of donor fluorescence during TbQSOX oxidation of DTT. Upon DTT injection, labeled enzyme rapidly converts to a state showing greater FRET efficiency (upper right panel). Other panels show longer time scales at various initial DTT concentrations. At starting DTT above ~200 μM (left panel), oxygen becomes limiting, the flavin becomes trapped as $FADH_2$ (see Fig. 1a), flavin absorbance at ~450 nm drops dramatically, and donor fluorescence increases correspondingly. At starting DTT concentrations of 200 μM or below (bottom right panel), DTT is limiting, and the enzyme returns to its oxidized, resting state.

$watermark-text
$watermark-text
$watermark-text

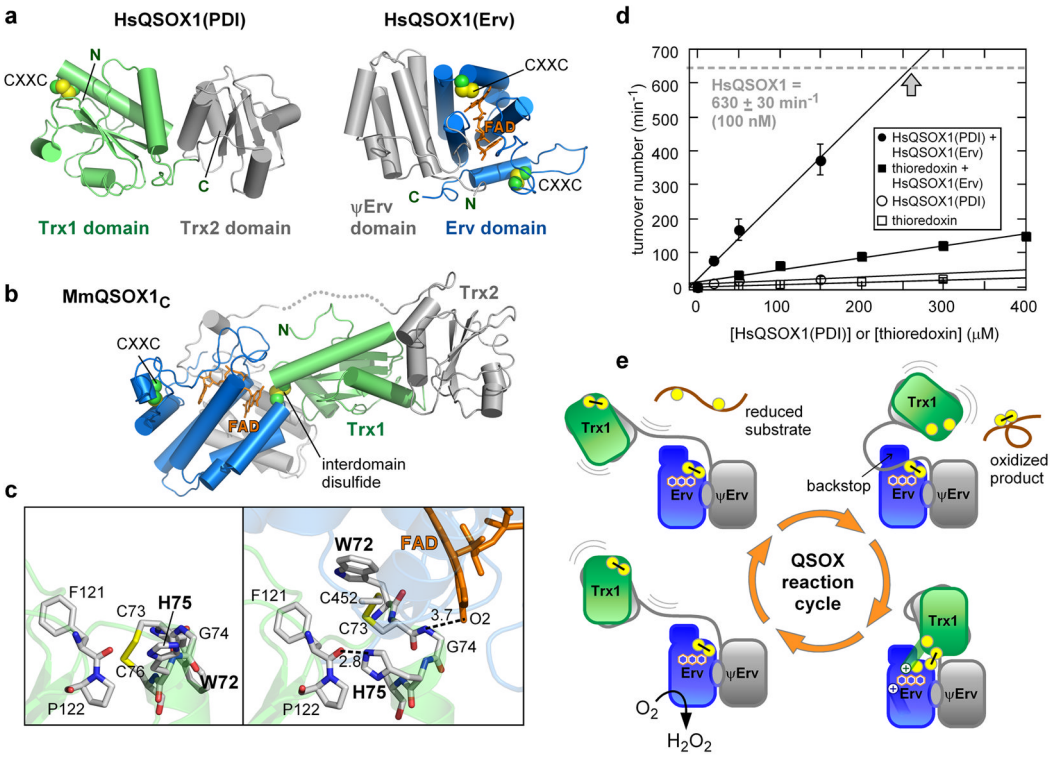

Figure 3. Mammalian QSOX and mechanistic insights into the QSOX catalytic cycle

a, The structures of HsQSOX1(PDI) (left) and HsQSOX1(Erv). Disulfides in CXXC motifs are shown. Other cysteines appear in Supplementary Fig. 13. **b**, Structure of $MmQSOX1_C$. **c**, Comparison of HsQSOX1(PDI) (left) with $MmQSOX1_C$ (right) shows rearrangements in the Trx1 redox-active region upon formation of the disulfide-transfer intermediate. Interatomic distances (dashed lines) are in Angstrom. **d**, Tethering increases the effective concentration of the HsQSOX1 disulfide transferring module. Initial oxygen consumption rates were recorded for 100 nM HsQSOX1(Erv) and varying concentrations of HsQSOX1(PDI) (filled circles) or thioredoxin (filled squares) upon injection of DTT. Gray, dashed line indicates the turnover number for intact HsQSOX1, measured at 100 nM. By extrapolation, ~250 μM HsQSOX1(PDI) with 100 nM HsQSOX1(Erv) would be expected to support a similar reaction rate (gray arrow). **e**, Summary of the structural basis of the QSOX catalytic mechanism, as revealed in this study. Adjacent yellow balls with black bar indicate disulfide bonds; separated yellow balls indicate reduced thiolates. The "+" symbols in the closed conformation (lower right) represent arginine side chains from either the Trx1 domain (in TbQSOX) or the Erv domain (in TbQSOX and mammalian QSOX1) that may contribute to the electron-withdrawing ability of the FAD. The "backstop" represents conserved Erv domain loops (Supplementary Fig. 9).

$watermark-text
$watermark-text
$watermark-text